SCIENCE CHINA
Chemistry

• ARTICLES •

January 2011 Vol.54 No.1: 223–230
doi: 10.1007/s11426-010-4130-9

Small-volume solution current-time behavior study for application in reverse iontophoresis-based non-invasive blood glucose monitoring

CHANG LingQian[1,2], LIU ChunXiu[1], HE YinZeng[1,2], XIAO HongHui[1,2] & CAI XinXia[1,2*]

[1]*State Key Laboratory of Transducer Technology; Institute of Electronics, Chinese Academy of Sciences, Beijing 100190, China*
[2]*Graduate University of Chinese Academy of Sciences, Beijing 100190, China*

Received March 20, 2010; accepted June 28, 2010; published online October 12, 2010

The reverse iontophoresis-based glucose monitoring circumstance is similar to the small-volume solution in which mass diffusion controls the current response of the electrochemical biosensors. In this study, the law of mass transfer in this type of solution was analyzed and a mathematic model was established to depict the current-time behavior of the fabricated planar electrode used in the non-invasive meter designed by ourselves. A small-volume glucose solution was directly constructed on the electrode to simulate the reverse iontophoresis-based sensing condition. The correctness of the model was demonstrated by chronoamperometry. Animal assay was subsequently carried out to verify the practicality of the model in determination of blood glucose. The results processed by the new method accurately traced the authentic value, confirming the advantage of the new method and the potential in clinical analysis.

non-invasive detection, current-time behavior, small-volume solution, mass transfer, semi-infinite diffusion, mathematic model

1 Introduction

Blood glucose monitoring has attracted much attention. In 2008, two reviews referring to glucose biosensors and diabetes management were published on *Chemical Reviews* [1, 2]. Commercial blood glucose biosensors mainly make use of two methods, including electrochemical approaches and optics. Among them, electrochemical test-strip plays a leading role for the advantages of requiring less than 4 μL finger blood and ensuring high clinical accuracy. However, it brings pain to diabetics for pricking skins. The ultimate goal of diabetes diagnosis is to use non-invasive ways to alleviate pain and to provide continuous monitoring [3]. In 1989, Guy's group established "reverse iontophoresis" [4–6], which demonstrated small molecules, such as tissue glucose, could be extracted through skins by imposing a couple of electrodes with small current on scarfskins. It enlightened one possibility of non-invasive glucose monitoring. Commercial GlucoWatch Biographer was subsequently developed based on this theory [7], but discontinued due to potential problems [1]. Recently, a new type of reverse iontophoresis-based blood sugar meter was developed by our group [8]. Compared to GlucoWatch, it has high performance on the glucose biosensor contributing to low power consumption and short warm-up time less than 30 min.

The two steps under reverse iontophoresis-based glucose monitoring system are extraction and sensing. Their progress orderly and eventually generate the current corresponding to the concentration of blood glucose. The osmosis kinetics of glucose drawn through skins is complex, leading to unclear rules established in early reports [9, 10]. The uncertainties of the extraction period may directly affect the next step, so effective analysis has the necessity of dividing the reverse iontophoresis system into two parts. When the monitoring process is analyzed, the extraction is

*Corresponding author (email: xxcai@mail.ie.ac.cn)

under control. In the present study, we focus on the current-time behavior of the fabricated biosensor used in this system. The extraction process was simulated by the following ways: We constructed a small-volume glucose solution on the electrode in order to make its configuration similar to the real reverse iontophoresis-based monitoring condition. The rationality of the simulation was demonstrated by the principle of the monitoring system as follows [7]: A couple of three-electrode biosensors are fastened to the skin. During detection, the space between the skin and the surface of the electrode (about hundreds of micrometers) is filled with small-volume buffer solution to enhance the mobility of extracted glucose to the electrode. The immobilized GO_x layer serves for collecting and catalyzing glucose.

The diffusion of glucose molecules in such small-volume solution was theoretically analyzed and a mathematic model was established to depict the current behavior. Then chronoamperometric measurement was performed with the fabricated electrode, and the current vs. time plots confirmed the correctness of the model. The animal experiment was subsequently processed using portable non-invasive blood glucose detection equipment invented by our group. The specimen was chosen from mini-pigs due to the similarities of skin structures between pig and human. The obtained curves demonstrated that the variation of porcine blood sugar could be precisely inspected by the mathematic model, according to the authentic values detected by the invasive method.

2 Experimental part and simulation

2.1 Reagents and apparatus

Glucose oxidase (GO_x, EC 1.1.3.4, 230 units/mg) was from Amresco, Japan. β-D-Glucose was purchased from Laibo Biology Inc., China. Poly(ethylene oxide) (PEO, average MW 600,000), phosphate buffer solution (PBS) containing 0.0027 M KCl, and 0.133 M NaCl (0.01 M, pH 7.4 at 25°C) were obtained from Sigma-Aldrich Inc., USA. Bovine serum albumin (BSA) and 25% glutaraldehyde solution were purchased from Yili Chemicals Inc., China. Silver/silver chloride (Ag/AgCl) ink was from Dupont Corp, USA. The poly-(vinylpyridine) complex of $Os(bpy)_2Cl$ wiring horseradish peroxidase, designated as HRP-PVP-Os, was synthesized by partially complexing the pyridine nitrogens of poly(4-vinylpyridine) with $Os(bpy)_2Cl^{+1/+2}$ according to the previously published reports [11, 12]. All the other reagents were of analytical grade and used without further purification. All aqueous solutions were prepared with deionized water.

The electrochemical measurements were performed at room temperature (25 °C) with a CHI660A electrochemical workstation (CH Instruments, USA). Microsoft Office Excel 2003 and MATLAB 7 were used for analyzing the experimental data.

2.2 Biosensor fabrication

For commercial purpose, the biosensors (conventional three-electrode systems) were mass-produced with a vacuum sputtering machine (H46500-4, Nanguang Machine Factory, China) by sputtering gold on a polyethylene terephthalate (PET) substrate, and then were cleaned by a plasma cleaner (Harrick Scientific Corp., USA) to enhance the electroactivity.

The reference electrode and the auxiliary electrode were simultaneously printed by Ag/AgCl ink for its strong stability in extraction, better than platinum as counter electrodes. The coated electrode was baked at 120 °C for 5 min. The gold working electrode was modified by dropping 4 μL HRP-PVP-Os solution onto the surface and stored for 3–5 days under ambient condition. The GO_x layer was constructed by entrapping glucose oxidase (10 μL, 10 units/μL) in 90 μL gel (consisting of 6 mg PEO as a gel-substrate for GO_x immobilization, 10 μL wt 20% bovine serum albumin, 8 μL glycerol as a humectant, 40 μL wt 1.25% glutaraldehyde as a cross-linking reagent, and 40 μL PBS), denoted as GO_x/HRP-PVP-Os electrode. The fabricated biosensor was dried and stored at 4 °C in a refrigerator.

2.3 Large-volume solution electrochemical measurement

To confirm whether the current response on the electrode was mass transfer limited, the electrochemical measurement was performed in a 15 mL glucose solution cell within which the biosensor was completely immersed. The electrode was linked to CHI660A used to measure the current vs. time plots. The measurement started with the potential 0.0 V vs. Ag/AgCl. Notably, it had been confirmed that 0.0 V was negative enough so that fast reactions happened at the electrode and the response current was limited by the mass transfer [11, 13, 14]. The current vs. time was measured every 0.1 second. The observed data were analyzed by Excel.

2.4 Simulation of the monitoring circumstance in reverse iontophoresis system and small-volume solution electrochemical measurement

The electrode was linked to the electrochemical workstation and its modified surface was exposed to the air. Before measurement, the gel layer was saturated with PBS in order to reduce double-layer charging. Subsequently 3 μL of glucose solution was dipped on the surface of the electrode and paved swiftly by the pipette. As shown in Figure 1, by this action, the configuration of the simulation was similar to the real monitoring circumstance of the reverse iontophoresis system. The measurement was subsequently started with 0.0 V. The data were analyzed by Excel and MATLAB 7.

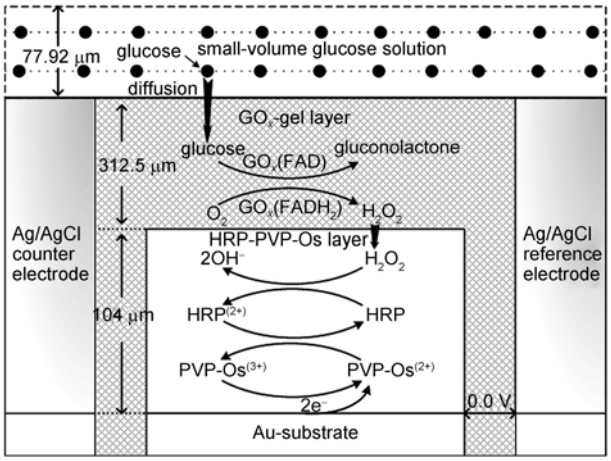

Figure 1 Schematic of the GO_x/HRP-PVP-Os electrode and the simulation of monitoring circumstance of the reverse iontophoresis system. The thickness of each layer was approximately calculated according to its volume and the electrode scale.

2.5 Animal experiment

The animal experiment was performed in Chinese Academy of Herbalist Science Attached Xiyuan Hospital. The specimen was chosen from Chinese experimental mini-pigs of 30 kg. The meter was fastened on the right belly of the pig which had been anesthetized by 3% amyl barbiturate, as shown in Figure 2(a). The small-volume solution was constructed between porcine skin and the electrode (Figure 2(b)) by PBS. In each cycle of detection, the extraction time was set at 5 min and the detection was 100 s. The authentic values were acquired by a GlucoDr AGM2200 glucose meter (Allmedicus Company, Korea). The data were analyzed by Excel and MATLAB 7.

3 Mathematic model

Figure 1 also represents the reactions of the biosensor. It can be found after glucose molecules in small-volume solution diffused into the GO_x layer, 5 steps were taken to generate electrons [13, 15]:

$$GO_x\,(FAD) + \text{glucose} \rightarrow GO_x\,(FADH_2) + \text{gluconolactone} \quad (1)$$

$$GO_x\,(FADH_2) + O_2 \rightarrow GO_x\,(FAD) + H_2O_2 \quad (2)$$

H_2O_2 generates and diffuses into the PVP-Os mediator layer:

$$H_2O_2 + HRP \rightarrow HRP^{(2+)} + 2OH^- \quad (3)$$

$$HRP^{(2+)} + 2PVP\text{-}Os^{(2+)} \rightarrow HRP + 2PVP\text{-}Os^{(3+)} \quad (4)$$

$$2PVP\text{-}Os^{(3+)} + 2e^- \rightarrow 2PVP\text{-}Os^{(2+)} \quad (5)$$

As evidence from eqs. (1)–(5), electrochemical behavior on the GO_x/HRP-PVP-Os electrode is complex for existence of nernstian reaction coupled chemical reaction. Response time at the electrode is influenced by the redox reaction and mass transport [16].

However, it has been reported that the electron transfer was rapid due to high performance of the film, such as high electroactivity of substantial portion [17], high permeability [18], short transfer route of electrons [11, 13, 14, 19, 20], etc. In appropriate range of concentrations where the enzymic bioactivity was high enough so that the rate of chemical reaction is much faster than that of mass transfer, the current can be considered as diffusion controlled.

As shown in Figure 1, the initial thickness of small-volume solution signed as l is calculated of 77.92 μm, larger than $(D_m t)^{1/2}$ (D_m is obtained in 3.1) defined as the shortest distance satisfying semi-infinite diffusion [21], leading to semi-infinite diffusion of the glucose molecules. However, the structure of the small-volume solution in Figure 1 differs with the typical thin layer electrochemical cell on the open-up configuration [22–24]. The influence from solvent evaporation should be taken into account. The thickness of the solution, l, should be replaced by a decline function denoted as $l(t)$. In the entire measurement, the diffusion of glucose follows Fick's second law [25]:

$$\frac{\partial C_g(x,t)}{\partial t} = D_m\left[\frac{\partial^2 C_g(x,t)}{\partial x^2}\right] \quad (6)$$

where D_m is the mass diffusive coefficient. Herein, the two-gel layer where active molecules transferred led D_m to be slower than that it should be in solution; C_g is the glucose concentration. The initial time condition is

$$C_g(x,0) = C_g^* \quad (7)$$

where C_g^* is the initial concentration of glucose solution. The boundary condition of the electrode surface is

$$C_g(0,t) = 0 \quad (8)$$

The other boundary is determined by the solution thick-

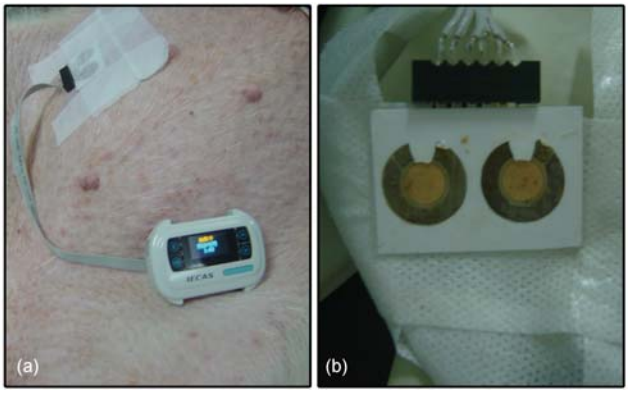

Figure 2 Photograph of installation of the detection system in animal experiment (a) and details of the planar glucose biosensors (b).

ness. As analyzed above, when t is small, semi-infinite diffusion is dominant for $l(t) > (D_m t)^{1/2}$, so the boundary effect can be neglected, and the mass transfer is considered as semi-infinite diffusion [21] with its boundary condition represented in eq. (9). When t grows up, $l(t)$ becomes smaller whereas $(D_m t)^{1/2}$ increases. The small-volume effect strengthens and the thickness of solution should be taken into account (eq. (10)) [26].

$$C_g(l,t) = C_g^*;\ l > (D_m t)^{1/2} \tag{9}$$

$$C_g(l(t),t) = 0;\ l(t) < (D_m t)^{1/2} \tag{10}$$

After Laplace transform, left term of the eq. (6) can be transformed to

$$\int_0^\infty \frac{\partial C_g(x,t)}{\partial t} e^{-st}\mathrm{d}t = -C_g^* + s\bar{C}_g(x,s) \tag{11}$$

Due to coexistence of two effects, right term of eq. (6) is divided into two parts. After transformation of Laplace:

$$\begin{aligned} & D_m \int_0^\infty \frac{\partial^2 C_g(x,t)}{\partial x^2} e^{-st}\mathrm{d}t \\ &= D_m \frac{d^2 \bar{C}_g(x,s)}{\mathrm{d}x^2} \\ &= D_m \left(\kappa_1 \frac{d^2 \bar{C}_g(x,s)}{\mathrm{d}x^2} + \kappa_2 \frac{d^2 \bar{C}_g(x,s)}{\mathrm{d}x^2} \right) \end{aligned} \tag{12}$$

where κ_1, κ_2 are factors influenced by eqs. (9) and (10). $\kappa_1 + \kappa_2 = 1$. Then

$$\kappa_1 \bar{C}_g(x,s) = \kappa_1 \left(\frac{C_g^*}{s} + C_1 e^{-\left(\frac{s}{D_g}x\right)^{1/2}} + C_2 e^{\left(\frac{s}{D_g}x\right)^{1/2}} \right) \tag{13}$$

$$\kappa_2 \bar{C}_g(x,s) = \kappa_2 \left(\frac{C_g^*}{s} + C_1 e^{-\left(\frac{s}{D_g}x\right)^{1/2}} + C_2 e^{\left(\frac{s}{D_g}x\right)^{1/2}} \right) \tag{14}$$

Eq. (13) under the semi-infinite boundary condition with $C_g(l,t) = \lim_{x\to\infty}(x,t) = C_g^*$ derives:

$$\kappa_1 C_g(x,t) = \kappa_1 C_g^* \mathrm{erf} \frac{x}{2D_m^{1/2} t^{1/2}} \tag{15}$$

To eq. (14), using eq. (10) as boundary condition:

$$\begin{aligned} \kappa_2 C_g(x,t) = \kappa_2 & \frac{4C_g^*}{\pi} \sum_{m=1}^{\infty} \left(\frac{1}{2m-1} \right) \\ & \cdot \exp\left[\frac{-(2m-1)^2 \pi^2 D_m t}{l(t)} \right] \sin\left[\frac{(2m-1)\pi x}{l(t)} \right] \end{aligned} \tag{16}$$

where m is exponential cofactor caused by Laplace transform. Diffusion-limited current is received:

$$\begin{aligned} i(t) = & \kappa_1 \frac{nFA_m D_m^{1/2} C_g^*}{\pi^{1/2}} t^{-1/2} \\ & + \kappa_2 \frac{4nFD_m C_g^*}{l} \sum_{m=1}^{\infty} \exp\left[\frac{-(2m-1)^2 \pi^2 D_m t}{l(t)^2} \right] \end{aligned} \tag{17}$$

where n, F have their usual significance; A_m is the geometric area of the work electrode. For long experimental time, terms of $m > 2$ can be omitted and an approximate equation yields,

$$\begin{aligned} i(t) = & \kappa_1 \frac{nFA_m D_m^{1/2} C_g^*}{\pi^{1/2}} t^{-1/2} \\ & + \kappa_2 \frac{4nFA_m C_g^* D_m}{\pi l} \exp\left(-\frac{\pi^2 D_m}{l(t)^2} t \right) \end{aligned} \tag{18}$$

$l(t)$ in eq. (18) is mathematical model about time dependence of the evaporative flux in a liquid-air system which recently was established by D.V. Alexandrov whose theory is based on the diffusion equation under the boundary condition [27]:

$$C \frac{\mathrm{d}l_\mathrm{V}}{\mathrm{d}t} = -D \frac{\partial C}{\partial \xi} + \alpha C, \quad \xi = l_\mathrm{V}(t),\ t > 0 \tag{19}$$

where C is the concentration of solvent; D is the diffusivity of the solvent; l_V is the vaporize thickness of the liquid; α is evaporation rate coefficient. Since the solvent con- centration distribution is assumed homogeneous throughout the experiment, eq. (19) can be highly simplified (eq. (20)), and expression of $l_\mathrm{V}(t)$ is obtained in eq. (21),

$$C \frac{\mathrm{d}l_V}{\mathrm{d}t} = \alpha C \tag{20}$$

$$l_\mathrm{V}(t) = \alpha t, \quad t > 0 \tag{21}$$

Therefore, the residual thickness of the small-volume can be given,

$$l(t) = l - l_\mathrm{V}(t) = l - \alpha t, \quad t > 0 \tag{22}$$

Substituting into eq. (22) leads to the equation,

$$\begin{aligned} i(t) = & \kappa_1 \frac{nFA_m D_m^{1/2} C_g^*}{\pi^{1/2}} t^{-1/2} \\ & + \kappa_2 \frac{4nFA_m C_g^* D_m}{\pi l} \exp\left(-\frac{\pi^2 D_m}{(l-\alpha t)^2} t \right) \end{aligned} \tag{23}$$

Since the decline rate of $l - \alpha t$ is much slower than that of current showing exponential decay, we are allowed to use its initial value, l, instead of eq. (22). The approximate equation yields,

$$i(t) = \kappa_1 \frac{nFA_m D_m^{1/2} C_g^*}{\pi^{1/2}} t^{-1/2} + \kappa_2 \frac{4nFA_m C_g^* D_m}{\pi l} \exp\left(-\frac{\pi^2 D_m}{l^2} t \right) \tag{24}$$

The model takes advantages of compatibility with Cottrell Equation under semi-infinite boundary and the thin layer electrochemical model. When $\kappa_1 = 1$, $\kappa_2 = 0$, meaning the ratio of the volume of solution to electrode area is large enough so that this model can be treated as semi-infinite diffusion [28], thus eq. (24) equals to Cottrell equation; when $\kappa_1 = 0$, $\kappa_2 = 1$, it can be completely treated as thin layer electrolysis [29–31]. κ_1, κ_2 are variables dependent on initial thickness of solution and concentration distribution of electroactive species.

4 Results and discussion

4.1 Large-volume solution current-time behavior of the GO_x/HRP-PVP-Os electrode

Figure 3 shows the large-volume solution current vs. time plots of the electrode at different concentrations. It can be observed that the current decline rapidly in initial and keep stable after 40 s at the concentration range studied. Distinct gradients proportional to the concentrations are observed. Fitting results by i vs. $t^{-1/2}$ are shown in inset of Figure 3. Good linearity can be obtained between 1 and 100 s with the lowest R^2 of 0.9847, indicating that the reaction on the electrode is active and the current are controlled by mass-diffusion [15–17]. Evidently, the current response on the investigated electrode obeys Cottrell equation under the semi-infinite boundary [28]:

$$i(t) = \frac{nFA_m D_m^{1/2} C_g^*}{\pi^{1/2}} t^{-1/2} \quad (25)$$

The concentration range was 5–100 μM. By eq. (25), we obtained the detection sensitivity of 15.75 nA μM^{-1} cm^{-2}, and D_m of 0.94 × 10^{-6} cm^2 s^{-1}. Because of the influence from gel layer, it was smaller than theoretical value of 6.7 × 10^{-6} cm^2 s^{-1}, yet experimental curves demonstrated the semi-infinite diffusion of glucose could be guaranteed in 5–100 μM.

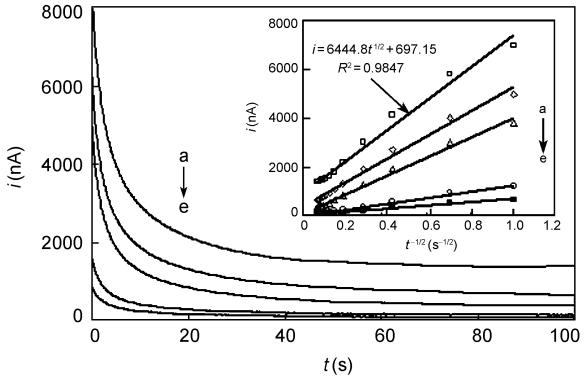

Figure 3 Large-volume solution current response of the fabricated electrode in (a) 100 μM, (b) 50 μM, (c) 20 μM, (d) 10 μM, (e) 5 μM glucose solution. Inset represents the fitting plots of i vs. $t^{-1/2}$ at concentrations of (a)–(e) with the time window of 1–100 s. Inserted equation and square of relativity coefficient belong to the plot of 100 μM concentration.

4.2 Small-volume solution current-time behavior of the GO_x/HRP-PVP-Os electrode

GlucoWatch reported that the extracted glucose concentrations were several orders of magnitude lower than those presented in the blood (~5 μM vs. ~5 mM) [7, 32, 33]. Our previous work also confirmed the detection linear range of the investigated electrode was 2–600 μM, being competent in reverse iontophoresis system (about 5–100 μM drawn glucose) [34]. Figure 4 represents the current vs. time plots of the electrode in constructed small-volume glucose solution. It can be found that the curves display similar trend in first 10 s. High relativity of $i(t)$ vs. $t^{-1/2}$ can be obtained in Figure 5 with the lowest R^2 of 0.9974, confirming that the semi-infinite mass diffusion is dominant in 1–10 s. Inset of Figure 4 shows current continue declining until their values are below background of 50 nA, indicating glucose molecules in the solution have been electrolyzed out. The

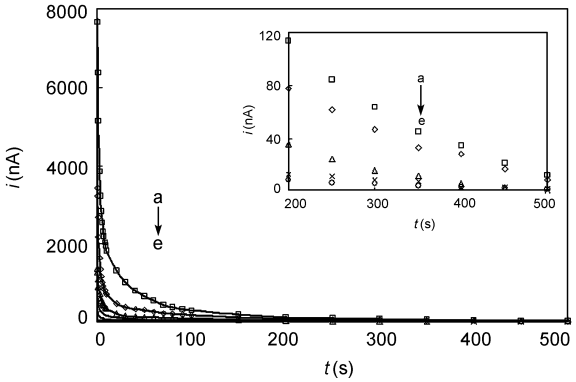

Figure 4 Small-volume solution current response of the fabricated electrode in (a) 100 μM (□), (b) 50 μM (◊), (c) 20 μM (Δ), (d) 10 μM (×), (e) 5 μM (○) glucose solution. Inset shows attenuation details of current after 200 s.

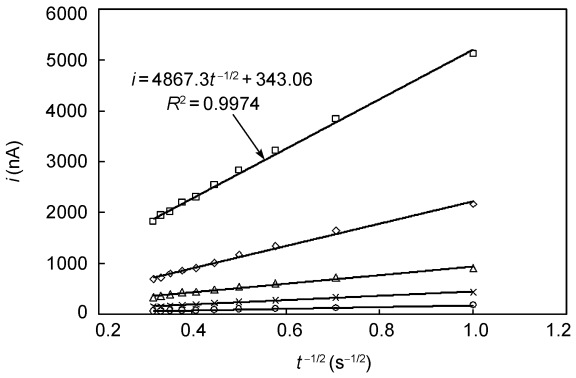

Figure 5 Fitting curves of i vs. $t^{-1/2}$ at concentrations of (○) 5 μM, (×) 10 μM, (Δ) 20 μM, (◊) 50 μM, (□) 100 μM small-volume glucose solution with the time windows of 1–10 s.

depletion phenomenon supports the rationality of the simulation, according to the report from GlucoWatch that extraction for 3 min and detection for 7 min during which the concentration of H_2O_2 consumed to near zero [7], implying electrolysis was completed.

The experimental data (black dots) were fitted by three models, as shown in Figure 6. Time windows were set from 10 to 300 s. As dashed-dots lines are results fitted by eq. (25), it can be obviously found semi-infinite diffusion curves trace beneath the experimental curves in the first 50 s, then turn over and keep stable. The residual values outweigh background current. The reasons for the disagreement have been analyzed before. Firstly, the initial thickness of the small-volume solution is larger than $(D_m t)^{1/2}$ of 30.7 μm with t =10 s, D_m = 0.94×10^{-6} cm^2 s^{-1}. Then the requirement of semi-infinite diffusion is dissatisfied due to gradual enhancement of $(D_m t)^{1/2}$. Secondly, the thickness of the solution lessens for evaporation, which makes dissatisfaction augment. Yet the rate of evaporation is much lower than that of electrolysis [27], so the complete electrolysis of glucose can be realized. The dashed lines represent the results fitted by typical thin-layer chronoamperometric equation which had been established by Hubbard and Anson [30], as shown in eq. (26).

$$i(t) = \frac{4nFA_m D_m C_g^*}{l} \exp\left(-\frac{\pi^2 D_m}{l^2} t\right) \approx i(0)\exp(-pt) \quad (26)$$

In this model, p is 0.0486 when l = 77.92 μm. It is observed that the model takes the advantage of expressing the depletion phenomenon of glucose, for the current declines into background in finite time [35, 36]. Due to the semi-infinite diffusion, eq. (26) fits original data poorly in the first 50 s. The data fitted by the small-volume solution diffusion-limited model were shown as the solid lines. p is calculated of 0.0486 by the initial value of l. This model complies well with the experimental data with high R^2. For instance, 0.9864 was obtained in 100 μM, higher than eq. (25) of 0.8708 and eq. (26) of 0.7608. κ_1 and κ_2 are dispensable variables in practical blood glucose measurement, so the investigation to acquire the precise expressions is not continued.

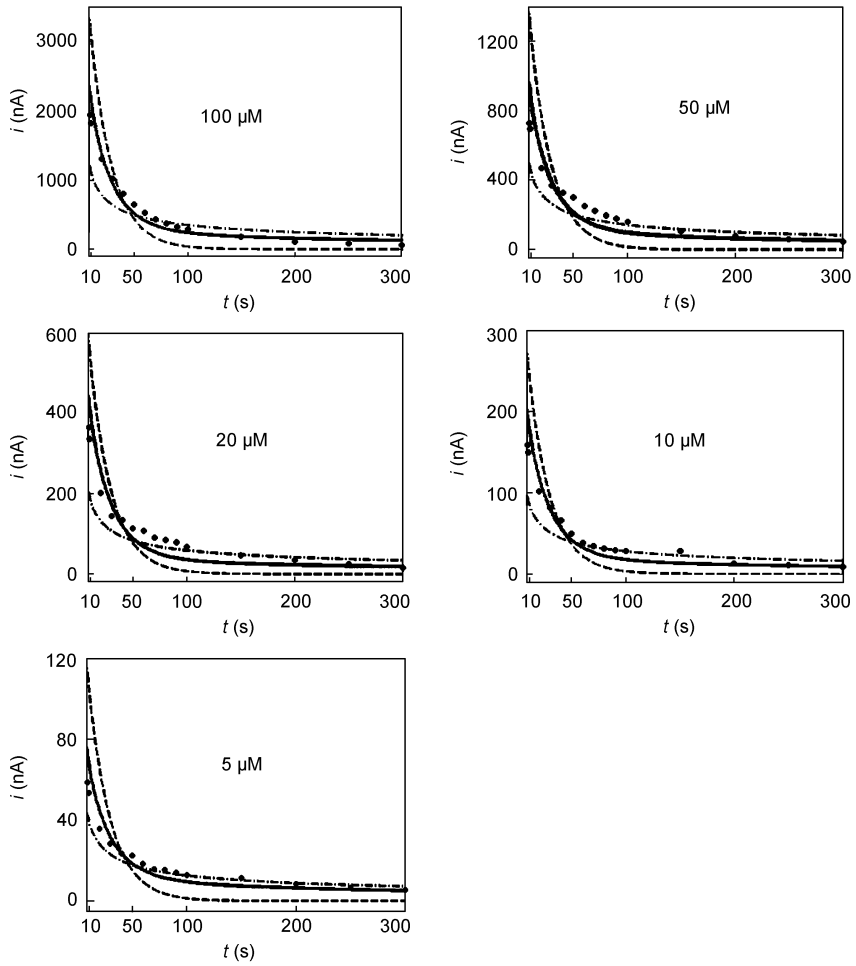

Figure 6 Results of experimental data (black dots) in the small-volume glucose solution fitted by eq. (25) (dashed-dots lines), eq. (26) (dashed lines) and eq. (24) (solid lines). Parameters p in eqs. (26) and (24) were calculated with l = 77.92 μm, D_m = 0.94×10^{-6} cm^2 s^{-1}.

4.3 Animal experimental results

Figure 7 represents current vs. time plots in animal experiment. After 5 min of extraction, the meter kept sensing for 100s until the obtained current decayed into background value of 50 nA. The experimental data (black dots) were fitted by three models. It can be seen that the curve fitted by the new model (solid lines) complied much better with the original data than those fitted by the semi-infinite model (dashed-dots lines) and the thin layer model (dashed lines). Because of the difference in the initial thickness of the solution, the curves at animal experiment appeared a little different with simulation assay curves. New method used to calculate blood sugar value was deduced from eq. (24). According to the equation, the term of κ_2 as influential portion could lead the exponent in $i(t) \sim t^{-1/2}$ to depart from −1/2 when the equation $i(t) \sim t^{-x}$ was adopted to fit the experimental curve. x was directly proportional to blood glucose concentration. Based on the consideration, new method used x in $i(t) \sim t^{-x}$ as contrast to indicate the trend of blood glucose. As shown in Figure 8, reverse iontophoresis based non-invasive method complies well with the fluctuation of porcine blood glucose, according to invasive detection.

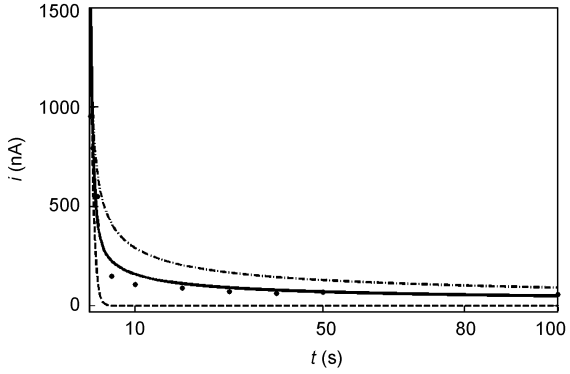

Figure 7 Results of obtained data (black dots) in one time of animal experimental fitted by eq. (25) (dashed-dots lines), eq. (26) (dashed lines) and eq. (24) (solid lines).

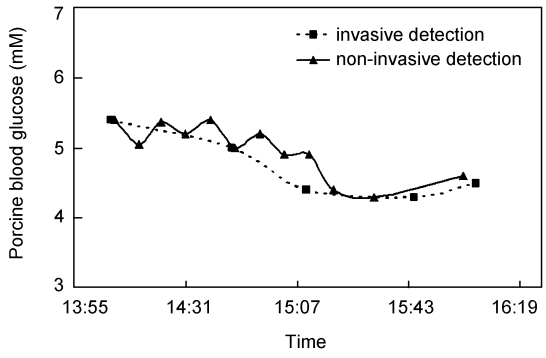

Figure 8 Fluctuation of porcine blood glucose detected by the non-invasive method (triangle lines) in comparison with the authentic value by invasive detection (rectangle lines) in one continuous monitoring.

5 Conclusions

In the present study, the mathematic model of mass transfer in small-volume solution was established with the aim to improve the precision and stability of reverse iontophoresis based non-invasive glucose detection. A simulation experiment was designed to simulate the detection environment in reverse iontophoresis system. Through the experiment, the correctness of the model was demonstrated. The animal experiment was subsequently performed, and the results confirmed the capability of the model in enhancing the precision and stability of non-invasive blood glucose monitoring. Human assay is underway to accumulate clinical data. Medical Clark errors grid used for evaluating the precision of the non-invasive glucose detection meter is about to be established.

The work was sponsored by Hi-Tech R. & D. Program of China (2007AA042105 & 2007AA04Z326) and CAS Innovative Program (KGCX2-YU-916).

1 Heller A, Feldman B. Electrochemical glucose sensors and their applications in diabetes management. *Chem Rev*, 2008, 108: 2482–2505
2 Wang J. Electrochemical glucose biosensors. *Chem Rev*, 2008, 108: 814–825
3 Pickup JC, Hussian F, Sachedina N. *In vivo* glucose monitoring: the clinical reality and the promise. *Biosens Bioelectron*, 2005, 20: 1897–1902
4 Glikfeld D, Hinz RS, Guy RH. Non-invasive sampling of biological fluids by ionphoresis. *Pharm Res*, 1989, 6: 988–990
5 Rao G, Glikfeld P, Guy RH. Reverse iontophoresis: development of a non-invasive approach for glucose monitoring. *Pharm Res*, 1993, 10: 1751–1755
6 Santi P, Guy RH, Reverse iontophoresis—Parameters determining electroosmotic flow: I. pH and ionic strength. *J Control Release*, 1996, 38: 159–165
7 Tierney MJ, Tamada JA, Potts RO, Jovanovic J, Gary S. Cygnus Research Team. Clinical evaluation of the GlucoWatch® biographer: a continual, non-invasive glucose monitor for patients with diabetes. *Biosens Bioelectron*, 2001, 16: 621–629
8 He YZ, Yang QD, Liu HM, Liu J, Cai XX. Research on electrochemical based wrist type non-invasive blood glucose monitor. Chinese Biomedicine Engineering Annual Conf. 09, Chongqing, China, 2009. 10
9 Marro D, Guy RH, Begona M. Characterization of the iontophoretic permselectivity properties of human and pig skin. *J Control Release*, 2001, 70: 213–217
10 Sekkat N, Naik A, Kalia YN, Glikfield P, Guy RH. Reverse iontophoretic monitoring in premature neonates: Feasibility and potential. *J Control Release*, 2002, 81: 83–89
11 Gregg BA, Heller A. Redox polymer films containing enzymes. 1. a redox-conducting epoxy cement: synthesis, characterization, and electrocatalytic oxidation of hydroquinone. *J Phys Chem*, 1991, 95: 5970–5797
12 Heller A. Electron-conducting redox hydrogels: Design, characteristics and synthesis. *Curr Opin Chem Biol*, 2006, 10: 664–672
13 Heller A. Electrlcal connection of enzyme redox centers to electrodes. *J Phys Chem*, 1992, 96: 3579–3587
14 Mano N, Mao F, Heller A. Electro-oxidation of glucose at an increased current density at a reducing potential. *Chem Commun*, 2004, 18: 2116–2117
15 Mikeladze E, Schulte A, Mosbach M, Blochl A, Csoregi E, Solomonia R, Schuhman W. Redox hydrogel-based bienzyme microelec-

trodes for amperometric monitoring of L-Glutamate. *Electroanalysis*, 2002, 14: 393–399
16 Andrieux CP, Audebert P, Bacchi P, Blohorn BD. Kinetic behaviour of an amperometric biosensor made of an enzymatic carbon paste and a Nation® gel investigated by rotating electrode studies. *J Electroanal Chem*, 1995, 394: 141–148
17 Rosca V, Popescu IC. Kinetic analysis of horseradish peroxidase "wiring" in redox polyelectrolyte-peroxidase multilayer assemblies. *Electrochem Commun*, 2002, 4: 904–911
18 Mano N, Mao F, Heller A. On the parameters affecting the characteristics of the "wired" glucose oxidase anode. *J Electroanal Chem*, 2005, 574: 347–357
19 Taylor C, Kenausis G, Katakis L, Heller A. "Wiring" of glucose oxidase within a hydrogel made with polyvinyl imidazole complexed with [(Os-4,4′-dimethoxy-2,2′-bipyridine) C1]$^{+/2+1}$. *J Electroanal Chem*, 1995, 396: 511–515
20 Degani Y, Heller A. Electrical communication between redox centers of glucose oxidase and electrodes via electrostatically and covalently bound redox polymers. *J Am Chem Soc*, 1989, 111: 2537–2358
21 Bard AJ, Faulkner LR. *Electrochemcial Methods: Fundmentals and Applications*. New York: Wiley Interscience, 2001. 453–455
22 Christensen CR, Anson FC. Chronopotentiometry in thin layers of solution. *Anal Chem*, 1963, 35: 205–209
23 Oglesby DM, Omang SH, Reilley CN. Thin layer electrochemical studies using controlled potential to controlled current. *Anal Chem*, 1965, 37: 1312–1326
24 Hubbard AT, Anson FC, in Electroanalytical Chemistry, 4, Bard AJ, Faulkner LR. *Electrochemical Methods: Fundamental and Applications*. New York: Marcel Dekker, 1970. 139-140
25 Bard AJ, Faulkner LR. *Electrochemical Methods: Fundamentals and Applications*. New York: Wiley Interscience, 2001, 149
26 Heineman WR, Anderson CW, Halsail HB, Hurst MM, Johnson JM, Kreishman GP, Norris BJ, Simone MJ, Su CH. *Advances in Chemistry*, vol.1. Washington: American Chemical Society, 1982, Ch.1
27 Alexandrow DV. Toward a theory of evaporation processes in liquid-solid systems. *J Exp Theor Phys*, 2009, 109: 451–454
28 Bard AJ, Faulkner LR. *Electrochemical Methods: Fundamentals and Applications*. New York: Wiley Interscience, 2001, 163–164
29 Bard AJ, Faulkner LR. *Electrochemical Methods: Fundamentals and Applications*. New York: Wiley Interscience, 2001, 452
30 Hubbard AT, Anson FC, in Electroanalytical Chemistry, 4, Bard AJ, Faulkner LR. *Electrochemical Methods: Fundamental and Applications*. New York: Marcel Dekker, 1970. 129–131
31 Schmidt E, Gygax HR. Gleichspannungspolarographie an. Kammarelektroden, Chimia, 1962, 16: 165–167
32 Garg SK, Fermi SJ, Potts RO, Tamada JA, Ackerman NR, Chase GP. Correlation of fingerstick blood glucose measurements with glucowatch biographer glucose results in young subjects with type 1 diabetes. *Diabetes Care*, 1999, 22: 1708–1714
33 Tierney MJ, Jayalakshmi Y, Parris NA, Reidy MP, Uheghu C, Vijayakumar P. Design of a biosensor for continual, transdermal glucose monitoring. *Clin Chem*, 1999, 45: 1681–1683
34 Liu HM, Liu CX, Jiang LY, liu J, Yang QD, Guo ZH, Cai XX, Osmium redox hydrogel mediated biosensor for measurement of low concentration glucose extracted by reverse iontophoresis. *Electroanalysis*, 2008, 2: 170–177
35 Regine D, Bergel A, Comtat M. Mass transfer with chemical reaction in thin-layer electrochemical reactors. *AIChE J*, 1995, 41: 1944–1954
36 Zhang CJ, Park SM. Simple technique for constructing thin-layer electrochemical cells. *Anal Chem*, 1988 60: 1639–1642